RSC Advances

ROYAL SOCIETY OF CHEMISTRY

www.rsc.org/advances

Probing molecular basis of single-walled carbon nanotube degradation and nondegradation by enzymes based on manganese peroxidase and lignin peroxidase

Ming Chen, [a,b,c] Xiaosheng Qin, [c,*] , Jian Li, [c] and Guangming Zeng [a,b]

[a]College of Environmental Science and Engineering, Hunan University, Changsha 410082, China

[b]Key Laboratory of Environmental Biology and Pollution Control (Hunan University), Ministry of Education, Changsha 410082, China

[c]School of Civil and Environmental Engineering, Nanyang Technological University, Singapore 639798

Keywords: carbon nanotube, biodegradation, enzyme, interaction, environmental remediation.

[*]Corresponding author: Dr. Qin Xiaosheng, School of Civil and Environmental Engineering, Nanyang Technological University, Singapore 639798; Tell: +65-67905288; Fax: +65-67921650; E-mail: xsqin@ntu.edu.sg

Abstract

Increasing evidence showed that carbon nanotubes (CNTs) presented adverse effects on the environment and human health, which largely stressed the importance of exploring CNT biodegradation. In this study, we described the molecular basis of single-walled carbon nanotube (SWCNT) biodegradation using a CNT-degrading enzyme (i.e. manganese peroxidase, MnP) and a CNT-nondegrading enzyme (i.e. lignin peroxidase, LiP) from *Phanerochaete chrysosporium* with similar catalytic cycles. Our results evidenced that SWCNT impeded the native conformational changes in free LiP by anchoring its loop regions to avoid the degraded fate. On the contrast, SWCNT did not limit conformational transitions in MnP and might induce larger conformational fluctuations than in free MnP by interacting with its helical and loop regions, providing the molecular basis of SWCNT degradation. SWCNT affected slightly the secondary structures and the mean smallest distances between residue pairs in LiP and MnP. These findings are useful for better understanding the biodegradation mechanism of CNTs, pre-estimating the biodegradation potential of CNTs and developing more promising CNT-degrading enzymes.

Introduction

Carbon nanotubes (CNTs) consisting of cylindrical graphite sheets exhibit diverse properties, including physical strength, light weight and electroconductivity [1-4]. Researchers have been stimulated to use CNTs in a wide range of fields such as environmental remediation [5-9], drug delivery agents, sensors [10-12], and hydrogen storage [13]. Despite wide applications, little is known about the structural dynamics of enzyme-CNT interactions when CNTs are subjected to different enzyme-catalyzed fates (degradation and nondegradation). Can molecular dynamics provide clues to enzyme-catalyzed fates of CNTs? Why do the same CNTs have different fates when facing enzymes with similar catalytic cycles at the molecular level? All these questions are yet to be answered.

Protein-CNT interaction mechanism remains largely unclear. In 2012, Calvaresi et al. pointed out that only a small number of studies investigated the protein-CNT interactions at a molecular level [14]. Probing enzyme-CNT interactions can broaden our understanding of protein-CNT interactions, as enzymes are protein in essence [15]. It has been observed that some proteins such as lysozyme interacted with CNTs [14, 16]. Shams et al. [17] investigated the interaction of actin with SWCNT through MD simulations, finding that actin formed hydrophobic interactions with SWCNT. To improve the understanding of protein-CNT interactions, He et al. probed the interactions of 20 standard amino acids with CNT, finding that four types of amino acids (i.e. Phe, Tyr, Trp and Arg) had the highest binding affinity for CNT [18].

Increasing use of CNTs and other pollutants in the society are bringing risks to the environment and human health [19-23]. Thus, it is necessary to remove and degrade CNTs released into the environment. Unfortunately, the high aspect ratio, the aromatic structure and the size of SWCNT make degradation of CNTs rather challenging [24]. It has been

demonstrated by several previous studies that biodegradation was a good choice for the removal of CNTs and other pollutants [25, 26]. Zhao et al. investigated the degradation of carboxylated and nitrogen-doped multiwalled carbon nanotubes (MWCNTs) by horseradish peroxidase with H_2O_2 [27]. After 80 days, carboxylated MWCNTs were partly degraded, while nitrogen-doped MWCNTs were decomposed completely. *Sparassis latifolia* mushroom could decompose the thermally-treated and raw grade carboxylated SWCNTs by lignin peroxidase (LiP) [28]. Lactoperoxidase from the airways together with H_2O_2 and NaSCN was capable of degrading oxidized SWCNTs with or without pulmonary surfactant [29]. SWCNTs were also found to be degraded by eosinophil peroxidase [30]. Interestingly, Zhang et al. studied the degrading potential of ligninolytic enzymes for SWCNTs [31]. They found that manganese peroxidase (MnP) from *Phanerochaete chrysosporium* could degrade pristine SWCNTs, but LiP from *P. chrysosporium* could not. MnP and LiP belong to heme-containing peroxidase, and have similar catalytic cycles [32, 33]. For efficient degradation of CNTs and in order to reduce the adverse impact of CNTs incautiously released into the working place on human health and the environment, it is necessary to explore the structural dynamics of CNT-degrading enzyme and CNT-nondegrading enzyme when interacting with the same CNT. Due to the similar properties and completely different catalytic effects on SWCNT for LiP and MnP from *P. chrysosporium*, they were a pair of ideal model systems for the present purpose.

In this study, we aim to analyze the interactions of CNT-degrading enzyme and CNT-nondegrading enzyme with the SWCNT by multiple molecular dynamics (MD) simulations using two ligninolytic enzymes-LiP and MnP as representatives. The distinction of structural dynamics between complexes of CNT with CNT-degrading enzyme and CNT-nondegrading enzyme could be helpful in estimating the potential for enzymatic decomposition of CNTs and developing more promising CNT-degrading enzymes.

Materials and methods

Molecular dynamics (MD) simulation gives a detailed overview of the interacting process between enzyme and SWCNT at a molecular level [14]. Comparison between LiP-SWCNT (LiP tends to nondegrade CNT [31]) and MnP-SWCNT (MnP tends to degrade CNT [31]) could provide the initial cues to enzyme-catalyzed fate of carbon nanotube, because binding is an initial step for enzymes' catalysis according to induced fit theory. The starting configurations of LiP-SWCNT and MnP-SWCNT were constructed using PatchDock, a molecular docking tool taking shape complementarity into account [34]. The best structures were further produced by FireDock [35]. PatchDock and FireDock have been confirmed useful to the docking of CNT to protein [14]. The crystal structures of LiP (PDB code: 1LLLP [36]) and MnP (PDB code: 3M5Q [37]) from *P. chrysosporium* were downloaded from Protein Data Bank [38]. Ligands and water molecular were removed from these enzyme structures. SWCNT (5,5) was constructed by Nanotube Builder of Visual Molecular Dynamics (VMD) [39].

We carried out separate simulations for LiP-water, LiP-SWCNT-water, MnP-water and MnP-SWCNT-water systems. The initial configurations were shown in Figure S1. Single enzyme or enzyme-SWCNT complexes were positioned at the center of a cubic box solvated with SPC water model. The side length of the box is 8.98788 nm for LiP-water and LiP-SWCNT-water systems, while it is 7.82558 nm for MnP-water and MnP-SWCNT-water systems. Gromacs 4.6 package [40, 41] was used to carry out MD simulations with OPLS-AA force field [42] under periodic boundary conditions. The systems were subjected to steep descent minimization with an energy step size of 0.01, followed by 400 ps of NVT and 400 ps of NPT simulations. The time step was 2 fs. Na^+ was added into solvated box to neutralize the systems. After equilibrium, a 30 ns-simulation was applied to explore the structural dynamics of LiP, MnP, LiP-SWCNT and MnP-SWCNT in water solution. The algorithms for

long-range electrostatics, holonomic constraints, temperature coupling and pressure coupling were Particle Mesh Ewald [43], LINCS [44], V-rescale [45] and Parrinello-Rahman [46], respectively. Temperature (300 K) and pressure (1 atm) were held constant during simulation. Trajectories and energies were saved every 10 ps.

Results

Our goals were to investigate the atomic level interactions of the same CNT with CNT-degrading enzyme and CNT-nondegrading enzyme. On this basis, we analyzed the molecular basis leading to different enzyme-catalyzed fates of CNT (degradation and nondegradation). We selected CNT (5,5) for the present purpose, which is consistent with the previous study done by Shams et al [17]. MD simulations were performed for enzyme-SWCNT complexes and the control groups that only contain enzymes to shed light on the conformational changes of simulated enzymes in the presence of the SWCNT.

Binding regions

The initial conformations of LiP-SWCNT and MnP-SWCNT were shown in Figure S1. SWCNT located only adjacent to loop regions of LiP, whereas SWCNT was positioned proximal to both α-helical and loop regions of MnP. We further extracted the binding conformations of LiP-SWCNT and MnP-SWCNT at 0 ns, 10 ns, 20 ns and 30 ns, showing that the characteristics of binding regions of LiP-SWCNT and MnP-SWCNT were consistent with those of initial ones, respectively (Fig. 1). Namely, LiP bound to SWCNT by loop regions, while MnP interacted with SWCNT using helices besides loop regions.

To observe the variations in binding regions of LiP and MnP to SWCNT during the simulation, we retained the residues within 3 Å of SWCNT. We termed the region consisting of these residues "3Å-region". We found that hydrophobic and hydrophilic residues were

always in 3Å-region of LiP at 0, 10, 20 and 30 ns, and that charged residues only disappeared at 10 ns (Fig. 2). Noteworthy, atoms in hydrophobic residues in 3Å-region were relatively more abundant than other types of residue atoms. Our study showed that LiP residues near the SWCNT were not fixed (Table S1). For example, at 0 ns, residues in 3Å-region were HIS30, PRO296, GLY297, ASN298, GLY299, PRO300, LEU328, PRO329, ILE338, PRO339, HIS341 and LYS342. After 10 ns, residues in 3Å-region became GLN33, GLY35, THR196, ILE199, PRO296, GLY297, GLY299, PHE303, LEU328, PRO329, ALA336 and ILE338. Interestingly, four residues (PRO296, GLY297, LEU328 and PRO329) were common at 0, 10, 20 and 30 ns, implying their important contribution to stabilizing the LiP-SWCNT interaction. Similarly, residues in 3Å-region of MnP also changed during the simulation (Fig. 3), whose types varied from 3 ARG, 2 ALA and 1 PHE at 0 ns to 1 ARG, 1 ALA, 2 PHE, 1 CYS, 1 ILE and 1 SER at 30 ns (Table S2). ARG8, PHE264 and ALA267 were always found in 3Å-region of MnP at 0, 10, 20 and 30 ns. Thus, it was inferred that these three residues were critical to the interaction of MnP with SWCNT. Generally, atoms in hydrophobic and charged residues in 3Å-region of MnP were more than those in hydrophilic residues.

Interaction energy

Interaction energies (sum of short range coulomb and short range Lennard-Jones energies) were estimated and were shown in Fig. 4. Mean interaction energies were -394.4 and -339.6 kJ/mol for LiP-SWCNT and MnP-SWCNT, respectively. Generally, the interaction energy of LiP-SWCNT was lower than that of MnP-SWCNT, and fluctuated within a narrow range. Fig. 4 showed that, unlike LiP-SWCNT, the interaction energy of MnP-SWCNT did not fleetly stabilize. The lowest and highest interaction energies of MnP-SWCNT were -443.704 and -

184.73 kJ/mol, respectively, implying a large fluctuation in interaction energies of MnP-SWCNT.

Conformational transitions

One of this study's focuses was to examine whether the dynamic behavior of CNT-degrading enzyme and CNT-nondegrading enzyme was different when they were subjected from the same SCWNT. Comparison between trends of LiP complexed with SWCNT and free LiP based on radius of gyration (Rg), Root-mean-square deviation (RMSD) and Root-mean square fluctuation (RMSF) showed that LiP did not keep its native conformation upon complexed with the SWCNT and become more stable (Fig. 5). However, MnP had an opposite tendency.

RMSD analysis indicated that SWCNT tended to stabilize the LiP conformation (average RMSD: 0.164 nm for LiP backbone with SWCNT and 0.201 nm for free LiP backbone), while MnP backbone RMSD exhibited a larger fluctuation (average RMSD=0.301 nm) and became more unstable than free MnP backbone (0.242 nm) in the presence of SWCNT. Rg, an indicator of structural compactness [26], showed a similar trend between free LiP and unfree LiP about 20 ns ago. After 20 ns, Rg of free LiP started to vary, but Rg of unfree LiP still followed its original trend. In other words, native conformational change in free LiP did not occur in unfree LiP due to the presence of SWCNT. By contrast, SWCNT almost did not affect the Rg pattern of MnP, because the Rg lines for MnP protein with and without SWCNT basically overlapped. RMSFs are often used to describe the residue flexibility in protein [26, 47]. C_α-RMSFs fluctuated remarkably around the regions consisting of residues 54-64, 175-191, 212-228 and 318-343 in free LiP during the simulation. These flexibilities were significantly reduced in LiP with SWCNT. Although the residue flexibility differed in MnP in the presence and absence of SWCNT, SWCNT did not inhibit the residue flexibility. Even

in some regions, such as residues 209-227, 341-349 and 356-357, SWCNT enhanced the residue flexibility in MnP.

Secondary structure and residue-residue distance

Secondary structures of LiP in the presence and absence of SWCNT were investigated to reveal how different secondary structures varied between them (Fig. 6). For residues 1-10, the secondary structure pattern in these two complexes almost did not vary in the first period; in the period between about 16000 and 20000 ps, the secondary structural composition was transformed into bend and coil and the structural composition afterwards became coil, bend, turn and 3-helix in free LiP. For residues 11-20, in the period between 17000-30000 ps, some residues tended to keep α-helix structure in free LiP, rather than turn structure in unfree LiP. For other regions of LiP, secondary structural transitions were also often observed. Another common feature for LiP with and without SWCNT was that α-helix, turn, bend and coil were relatively abundant structural forms.

Next we analyzed secondary structure plots of MnP with and without SWCNT (Fig. 6). In residues 1-50, secondary structure changes exhibited a similar pattern overall between unfree and free MnP with many minor differences. For example, secondary structures of residues 40-50 in free MnP changed frequently between turn and α-helix in the later stage of the simulation, but these residues' secondary structures in MnP with SWCNT varied very little and were α-helix in most of the simulation time. Some regions in MnP with and without SCWNT were conserved in secondary structures, such as the regions composed of residues 120-130. Turn, α-helix, bend and coil were relatively common secondary structural forms in MnP as observed in LiP. In summary, SWCNT affected the secondary structures of both LiP and MnP, leading to many local differences observed between free and unfree forms of LiP and MnP, respectively.

Fig. 7 showed the residue-residue contact maps based on mean smallest distance. We found that the contact map of LiP with SWCNT was similar to that of LiP without SWCNT. Only very small differences were found between them. The same was true for MnP with and without SWCNT.

Discussion

CNTs are acting as highly promising materials for wide applications in various fields, such as biosensors [48, 49] and environmental remediation [6, 50-52]. It was estimated that the demand for SWCNTs increased from 90 million US$ in 2009 to 600 million US$ in 2014 [19]. However, the increasing use of CNTs accelerated the probabilities of CNTs released into the environment. More and more studies showed that CNTs were toxic and posed significant threats to environment and human health [53]. For example, it has been reported that CNTs could bring various harmful impacts on human health, including cancer (e.g. skin and lung cancer), inflammation, mutagenicity, epithelioid granulomas and genotoxicity [19, 53]. It is thus desired that efficient technologies are developed for helping the removal of CNTs from the environment. In this regard, the application of biodegradation technology for CNTs has confirmed to be successful, as multiple types of enzymes have been found to have the ability to degrade CNTs from the previous studies, including MnP [31], horseradish peroxidase [27], lactoperoxidase [29], eosinophil peroxidase [30], *etc*. However, until now, no studies have investigated the molecular basis of CNT degradation and nondegradation by enzymes. In this study, we analyzed the effects of the same SWCNT (5,5) on structural dynamics in CNT-degrading enzyme (MnP) and CNT-nondegrading enzyme (LiP), looking for the initial clues to enzyme-catalyzed fates of CNTs through MD simulations. Previously, MD simulations have been confirmed to be an efficient method for the exploration of the interactions of CNTs with enzyme [14], DNA [4], antibodies [54], and other types of proteins [17].

Binding regions of SWCNT to LiP and MnP were different in secondary structure. SWCNT tended to be wrapped by the loop regions of LiP, and remained close to the loop and helical regions of MnP during the simulation (Fig. 1). Hydrophobic residues were generally more abundant than hydrophilic residues in 3Å-regions of SWCNT (Figs. 2 and 3). Shams et al. mentioned that the dominance of hydrophobic residues in contact with SWCNT might be attributed to the nonpolarity and electric neutrality of SWCNT [17]. In addition to hydrophobic residues, hydrophilic and charged residues also might contribute to the interactions of LiP and MnP with SWCNT. Our results showed that the interacting residues of LiP and MnP with SWCNT were not fixed during the simulation. Despite the high variations in these residues, some residues were always in 3Å-regions of SWCNT at 0, 10, 20 and 30 ns, including PRO296, GLY297, LEU328 and PRO329 of LiP and ARG8, PHE264 and ALA267 of MnP. We suggested these residues were potentially important to the interactions of SWCNT with LiP and MnP, respectively.

Native conformational variation in free LiP was impeded by the SWCNT based on RMSD, RMSF and Rg results (Fig. 5). According to induce fit theory [55, 56], conformational transition is necessary to enzymatic degradation. Thus, LiP was incapable of degrading SWCNT, as previously observed in experimental research [31]. In MnP-SWCNT, SWCNT did not prevent MnP from maintaining its native conformational changes. In addition, it appeared that SCWNT enhanced the conformational change in MnP on the basis of RMSD and RMSF results. This might be one of reasons why pristine SWCNT could be degraded by MnP in experimental study [31]. This finding related to different dynamic behavior of CNT-degrading and CNT-nondegrading enzymes in the presence of CNTs was useful for pre-estimation of the potential for enzymatic degradation of CNTs, selection of suitable enzymes or microbes for bioremediation of CNT-contaminated environment and design of more efficient CNT-degrading enzymes.

Interaction energy between LiP and SWCNT was generally lower than that between MnP and SWCNT (Fig. 4), implying a stronger LiP-SWCNT interaction. The strong interaction between SWCNT and CNT-nondegrading enzyme might have potential applications such as enzyme immobilization to enhance the stability and catalytic activity [57, 58].

An interesting phenomenon was the transitions in secondary structures and residue-residue mean smallest distance (Figs. 6 and 7). Dominant secondary structure forms were α-helix, turn, bend and coil in LiP and MnP regardless of whether SWCNT existed or not. SWCNT influenced the secondary structural patterns and residue-residue mean smallest distance in LiP and MnP, leading to slight differences between free and unfree proteins. These findings implied that SWCNT allowed minor secondary structural changes and reside fluctuations in CNT-nondegrading enzyme, although it impeded the native conformational transitions in CNT-nondegrading enzyme.

Conclusions

Our study results revealed the molecular basis of SWCNT degradation and nondegradation by enzymes through molecular dynamics. The SWCNT binding region located adjacent to helical and loop regions of MnP (a CNT-degrading enzyme) and loop regions of LiP (a CNT-nondegrading enzyme). PRO296, GLY297, LEU328 and PRO329 of LiP and ARG8, PHE264 and ALA267 of MnP were potentially important to the binding of SWCNT to LiP and MnP, respectively. Conformational transition in free CNT-nondegrading enzyme but not CNT-degrading enzyme was impeded by the presence of SWCNT. Our study is beneficial for understanding CNT-biodegrading mechanism and finding/developing more efficient enzymes for remediation of CNT-contaminated environment.

Conflicts of interest

The authors declare no competing financial interests.

Acknowledgments

The study was financially supported by the National Natural Science Foundation of China (51508177, 51521006), the Program for Changjiang Scholars and Innovative Research Team in University (IRT-13R17) and the Fundamental Research Funds for the Central Universities.

References

1. R. R. Johnson, A. C. Johnson and M. L. Klein, *Nano Lett*, 2008, 8, 69-75.
2. H. Liu, D. Nishide, T. Tanaka and H. Kataura, *Nat Commun*, 2011, 2, 309.
3. B. Pan, D. Zhang, H. Li, M. Wu, Z. Y. Wang and B. S. Xing, *Environ Sci Technol*, 2013, 47, 7722-7728.
4. D. Roxbury, J. Mittal and A. Jagota, *Nano Lett*, 2012, 12, 1464-1469.
5. X. Gui, Z. Zeng, Z. Lin, Q. Gan, R. Xiang, Y. Zhu, A. Cao and Z. Tang, *Acs Appl Mater Inter*, 2013, 5, 5845-5850.
6. S. Vadahanambi, S.-H. Lee, W.-J. Kim and I.-K. Oh, *Environ Sci Technol*, 2013, 47, 10510-10517.
7. V. K. Gupta, R. Kumar, A. Nayak, T. A. Saleh and M. Barakat, *Adv Colloid Interfac*, 2013, 193, 24-34.
8. J.-L. Gong, B. Wang, G.-M. Zeng, C.-P. Yang, C.-G. Niu, Q.-Y. Niu, W.-J. Zhou and Y. Liang, *J Hazard Mater*, 2009, 164, 1517-1522.
9. P. Xu, G. M. Zeng, D. L. Huang, C. L. Feng, S. Hu, M. H. Zhao, C. Lai, Z. Wei, C. Huang and G. X. Xie, *Sci Total Environ*, 2012, 424, 1-10.
10. S. Cui, H. Pu, G. Lu, Z. Wen, E. C. Mattson, C. Hirschmugl, M. Gajdardziska-Josifovska, M. Weinert and J. Chen, *Acs Appl Mater Inter*, 2012, 4, 4898-4904.

11. P. W. Barone, S. Baik, D. A. Heller and M. S. Strano, *Nat Mater*, 2005, 4, 86-92.
12. Q. Cao and J. A. Rogers, *Adv Mater*, 2009, 21, 29-53.
13. E. Tylianakis, G. K. Dimitrakakis, F. J. Martin-Martinez, S. Melchor, J. A. Dobado, E. Klontzas and G. E. Froudakis, *Int J Hydrogen Energ*, 2014, 39, 9825-9829.
14. M. Calvaresi, S. Hoefinger and F. Zerbetto, *Chem-Eur J*, 2012, 18, 4308-4313.
15. Q. Hu, P. S. Katti and Z. Gu, *Nanoscale*, 2014, 6, 12273-12286.
16. E. Wu, M. O. Coppens and S. Garde, *Langmuir*, 2015, 31, 1683-1692.
17. H. Shams, B. D. Holt, S. H. Mahboobi, Z. Jahed, M. F. Islam, K. N. Dahl and M. R. K. Mofrad, *Acs Nano*, 2014, 8, 188-197.
18. Z. J. He and J. Zhou, *Carbon*, 2014, 78, 500-509.
19. A. A. Shvedova, A. Pietroiusti, B. Fadeel and V. E. Kagan, *Toxicol Appl Pharm*, 2012, 261, 121-133.
20. G. Zeng, M. Chen and Z. Zeng, *Science*, 2013, 340, 1403-1403.
21. G. Zeng, M. Chen and Z. Zeng, *Nature*, 2013, 499, 154-154.
22. X. Qin, *Stoch Env Res Risk A*, 2012, 26, 43-58.
23. X. Qin, Y. Xu and J. Su, *Environ Eng Sci*, 2011, 28, 573-584.
24. T. D. Berry, T. R. Filley and R. A. Blanchette, *Environ Pollut*, 2014, 193, 197-204.
25. M. Chen, P. Xu, G. Zeng, C. Yang, D. Huang and J. Zhang, *Biotechnol Adv*, 2015, doi:10.1016/j.biotechadv.2015.1005.1003.
26. M. Chen, G. M. Zeng, C. Lai, J. Li, P. Xu and H. P. Wu, *Rsc Adv*, 2015, 5, 52307-52313.
27. Y. Zhao, B. L. Allen and A. Star, *J Phys Chem A*, 2011, 115, 9536-9544.
28. G. Chandrasekaran, S. K. Choi, Y. C. Lee, G. J. Kim and H. J. Shin, *J Ind Eng Chem*, 2014, 20, 3367-3374.

29. K. Bhattacharya, R. El-Sayed, F. T. Andon, S. P. Mukherjee, J. Gregory, H. Li, Y. C. Zhao, W. Seo, A. Fornara, B. Brandner, M. S. Toprak, K. Leifer, A. Star and B. Fadeel, *Carbon*, 2015, 91, 506-517.
30. F. T. Andón, A. A. Kapralov, N. Yanamala, W. Feng, A. Baygan, B. J. Chambers, K. Hultenby, F. Ye, M. S. Toprak and B. D. Brandner, *Small*, 2013, 9, 2721-2729.
31. C. Zhang, W. Chen and P. J. Alvarez, *Environ Sci Technol*, 2014, 48, 7918-7923.
32. T. D. Bugg, M. Ahmad, E. M. Hardiman and R. Rahmanpour, *Nat Prod Rep*, 2011, 28, 1883-1896.
33. Z. Huang, C. Liers, R. Ullrich, M. Hofrichter and M. A. Urynowicz, *Fuel*, 2013, 112, 295-301.
34. D. Schneidman-Duhovny, Y. Inbar, R. Nussinov and H. J. Wolfson, *Nucleic Acids Res*, 2005, 33, W363-W367.
35. E. Mashiach, D. Schneidman-Duhovny, N. Andrusier, R. Nussinov and H. J. Wolfson, *Nucleic Acids Res*, 2008, 36, W229-W232.
36. T. Choinowski, W. Blodig, K. H. Winterhalter and K. Piontek, *J Mol Biol*, 1999, 286, 809-827.
37. M. Sundaramoorthy, M. H. Gold and T. L. Poulos, *J Inorg Biochem*, 2010, 104, 683-690.
38. P. W. Rose, C. Bi, W. F. Bluhm, C. H. Christie, D. Dimitropoulos, S. Dutta, R. K. Green, D. S. Goodsell, A. Prlić and M. Quesada, *Nucleic Acids Res*, 2013, 41, D475-D482.
39. W. Humphrey, A. Dalke and K. Schulten, *J Mol Graph*, 1996, 14, 33-38.
40. B. Hess, C. Kutzner, D. Van Der Spoel and E. Lindahl, *J Chem Theory Comput*, 2008, 4, 435-447.

41. S. Pronk, S. Páll, R. Schulz, P. Larsson, P. Bjelkmar, R. Apostolov, M. R. Shirts, J. C. Smith, P. M. Kasson and D. van der Spoel, *Bioinformatics*, 2013, btt055.
42. G. A. Kaminski, R. A. Friesner, J. Tirado-Rives and W. L. Jorgensen, *J Phys Chem B*, 2001, 105, 6474-6487.
43. T. Darden, D. York and L. Pedersen, *J Chem Phys*, 1993, 98, 10089-10092.
44. B. Hess, H. Bekker, H. J. C. Berendsen and J. G. E. M. Fraaije, *J Comput Chem*, 1997, 18, 1463-1472.
45. G. Bussi, D. Donadio and M. Parrinello, *J Chem Phys*, 2007, 126.
46. M. Parrinello and A. Rahman, *J Appl Phys*, 1981, 52, 7182-7190.
47. K. M. Kumar, A. Anbarasu and S. Ramaiah, *Mol Biosyst*, 2014, 10, 891-900.
48. R. J. Chen, S. Bangsaruntip, K. A. Drouvalakis, N. W. S. Kam, M. Shim, Y. Li, W. Kim, P. J. Utz and H. Dai, *P Natl Acad Sci Usa*, 2003, 100, 4984-4989.
49. W. Yang, K. R. Ratinac, S. P. Ringer, P. Thordarson, J. J. Gooding and F. Braet, *Angew Chem Int Ed*, 2010, 49, 2114-2138.
50. W.-W. Tang, G.-M. Zeng, J.-L. Gong, Y. Liu, X.-Y. Wang, Y.-Y. Liu, Z.-F. Liu, L. Chen, X.-R. Zhang and D.-Z. Tu, *Chem Eng J*, 2012, 211, 470-478.
51. W.-W. Tang, G.-M. Zeng, J.-L. Gong, J. Liang, P. Xu, C. Zhang and B.-B. Huang, *Sci Total Environ*, 2014, 468, 1014-1027.
52. R. Kumar, M. A. Khan and N. Haq, *Crit Rev Env Sci Tec*, 2014, 44, 1000-1035.
53. C.-w. Lam, J. T. James, R. McCluskey, S. Arepalli and R. L. Hunter, *Crit Rev Toxicol*, 2006, 36, 189-217.
54. F. De Leo, J. Sgrignani, D. Bonifazi and A. Magistrato, *Chem-Eur J*, 2013, 19, 12281-12293.
55. D. E. Koshland, Jr., *P Natl Acad Sci Usa*, 1958, 44, 98-104.
56. P. Csermely, R. Palotai and R. Nussinov, *Trends Biochem Sci*, 2010, 35, 539-546.

57. A. P. Tavares, C. G. Silva, G. Dražić, A. M. Silva, J. M. Loureiro and J. L. Faria, *J Colloid Interf Sci*, 2015, 454, 52-60.

58. N. M. Mubarak, J. R. Wong, K. W. Tan, J. N. Sahu, E. C. Abdullah, N. S. Jayakumar and P. Ganesan, *J Mol Catal B-Enzym*, 2014, 107, 124-131.

Figure legends

Fig. 1. Snapshots of SWCNT interacting with LiP and MnP at 0, 10, 20 and 30 ns. 0 and 10 ns: front view; 20 and 30 ns: side view.

Fig. 2. Residue variation within 3 Å of SWCNT for LiP. Atoms in hydrophobic residues are colored in white, hydrophilic in green, and charged in red and blue.

Fig. 3. Residue variation within 3 Å of SWCNT for MnP. Atoms in hydrophobic residues are colored in white, hydrophilic in green, and charged in red and blue.

Fig. 4. Interaction energy as a function of the MD simulation time.

Fig. 5. Conformational transitions of LiP and MnP in the presence and absence of SWCNT. Left: LiP; Right: MnP.

Fig. 6. Changes in secondary structures of LiP (A, with SWCNT; B, without SWCNT) and MnP (C, with SWCNT; D, without SWCNT) during the simulation.

Fig. 7. Residue-residue contact maps of LiP (A, with SWCNT; B, without SWCNT) and MnP (C, with SWCNT; D, without SWCNT) based on mean smallest distance.

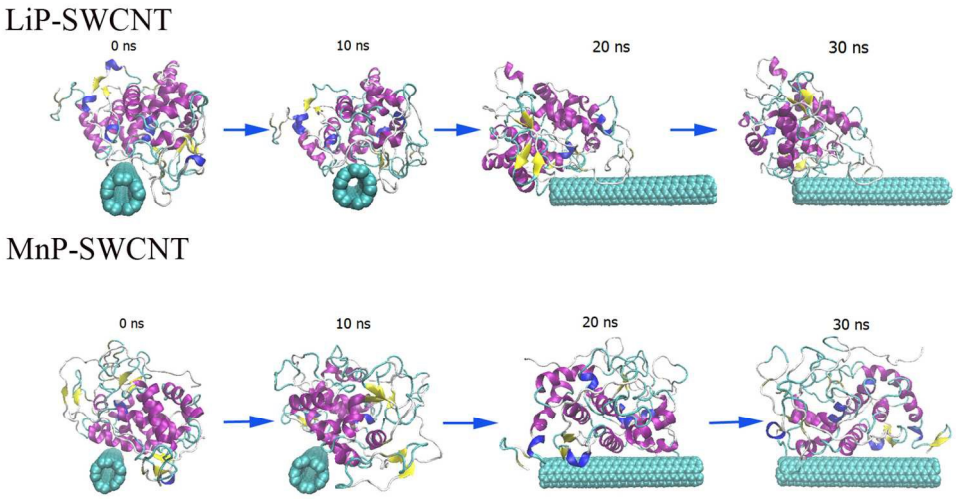

134x71mm (300 x 300 DPI)

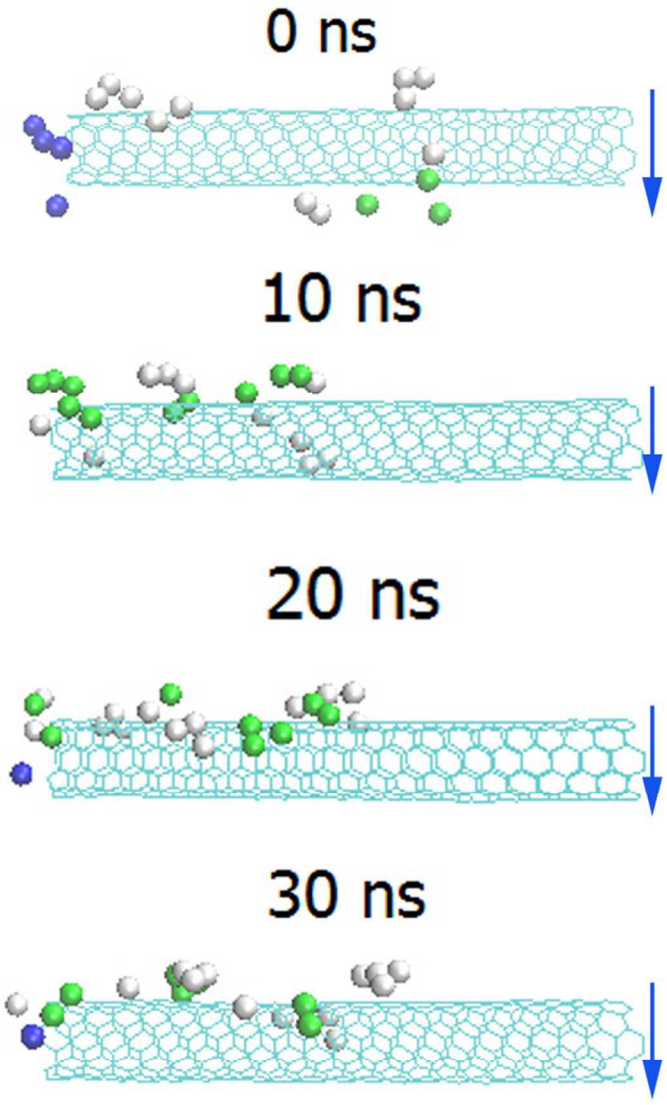

60x99mm (300 x 300 DPI)

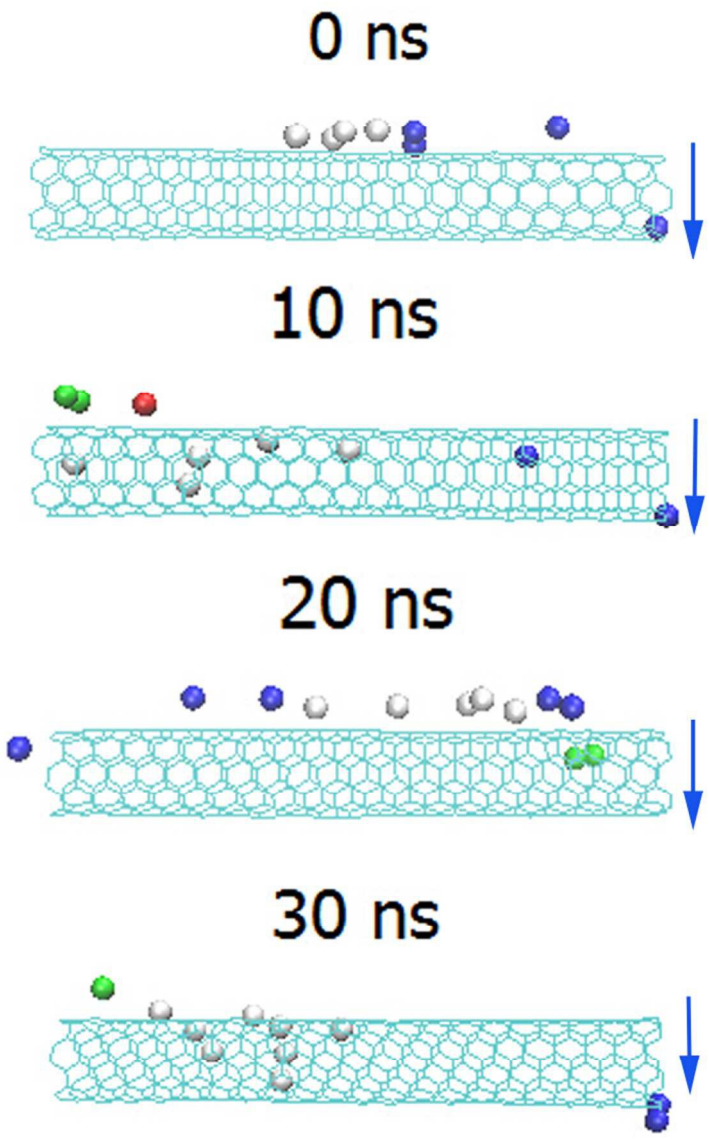

67x99mm (300 x 300 DPI)

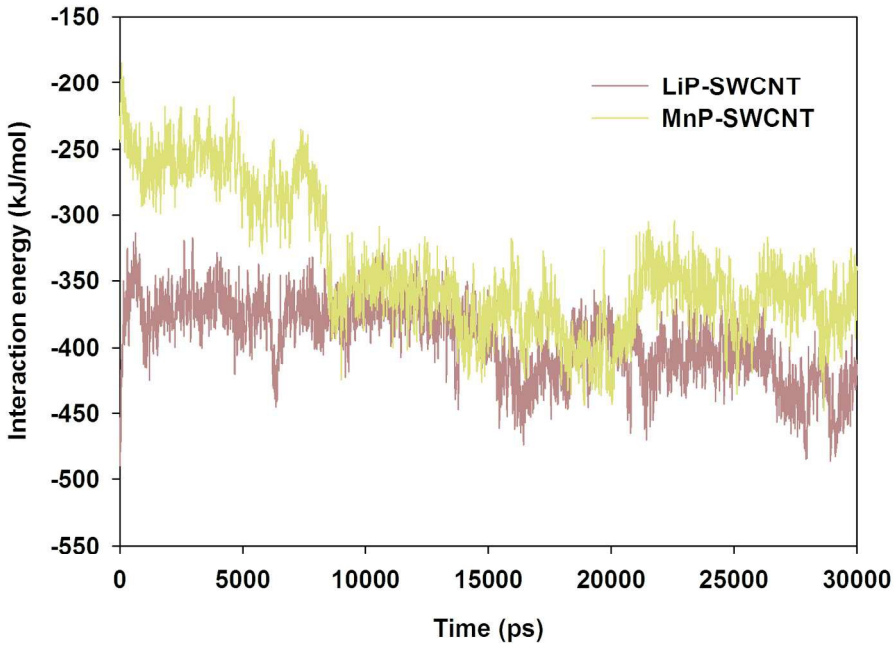

169x112mm (300 x 300 DPI)

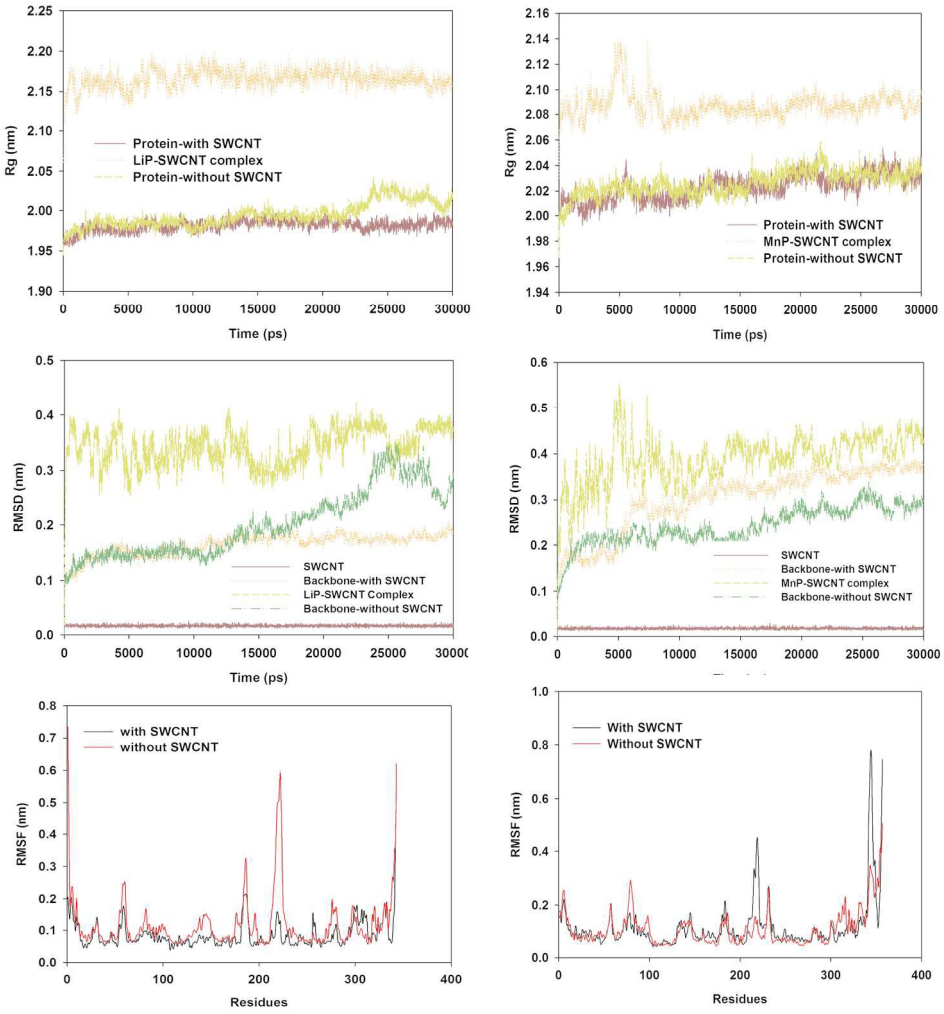

178x183mm (300 x 300 DPI)

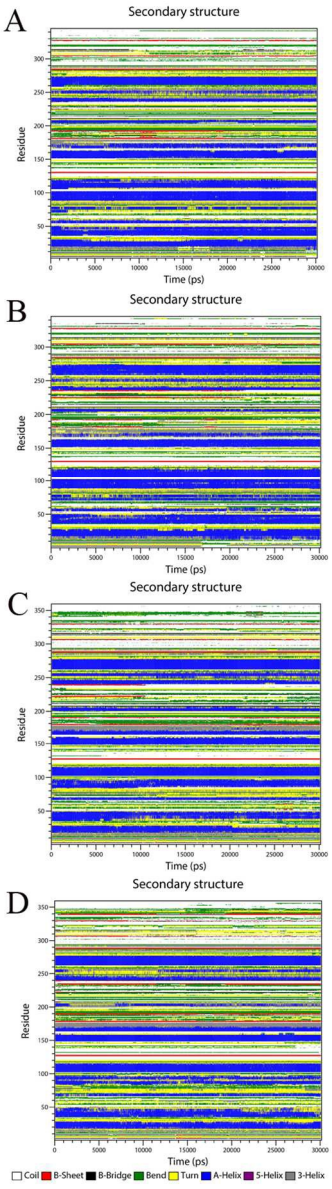

50x156mm (300 x 300 DPI)

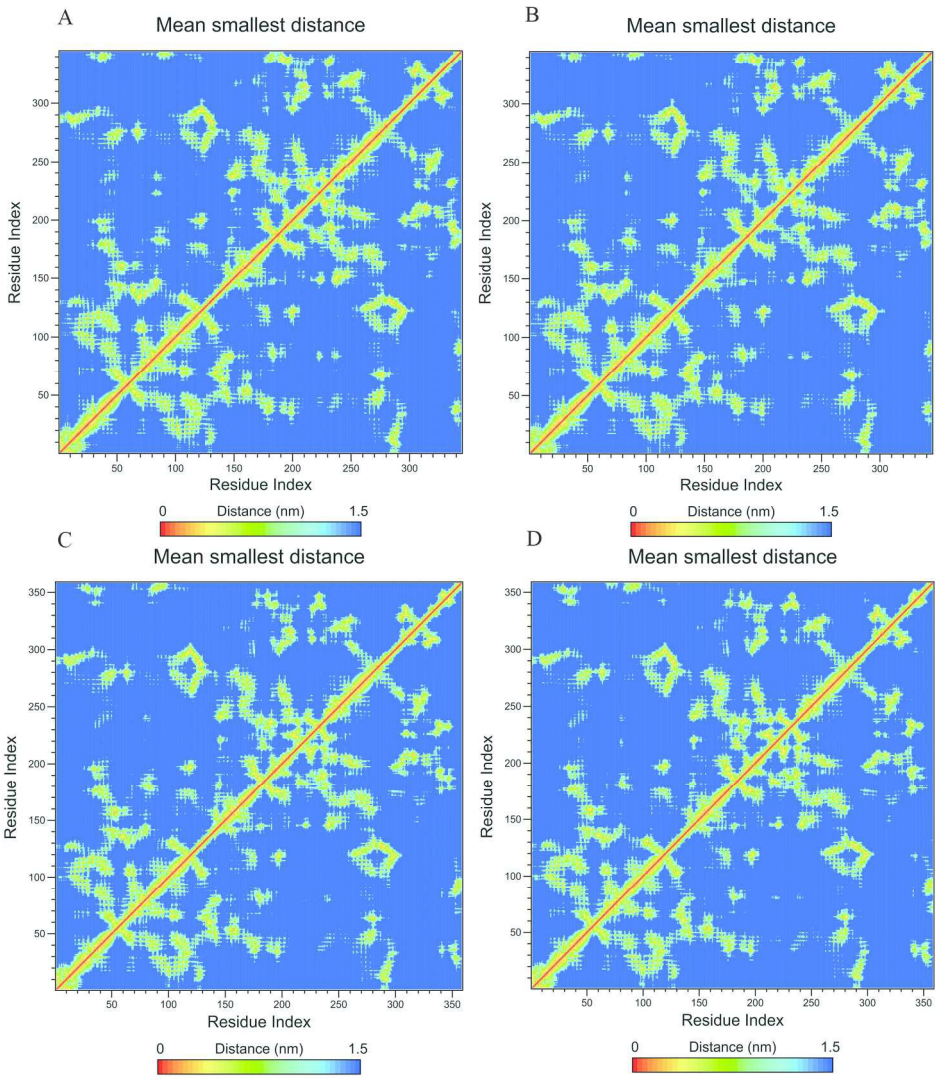

191x216mm (300 x 300 DPI)

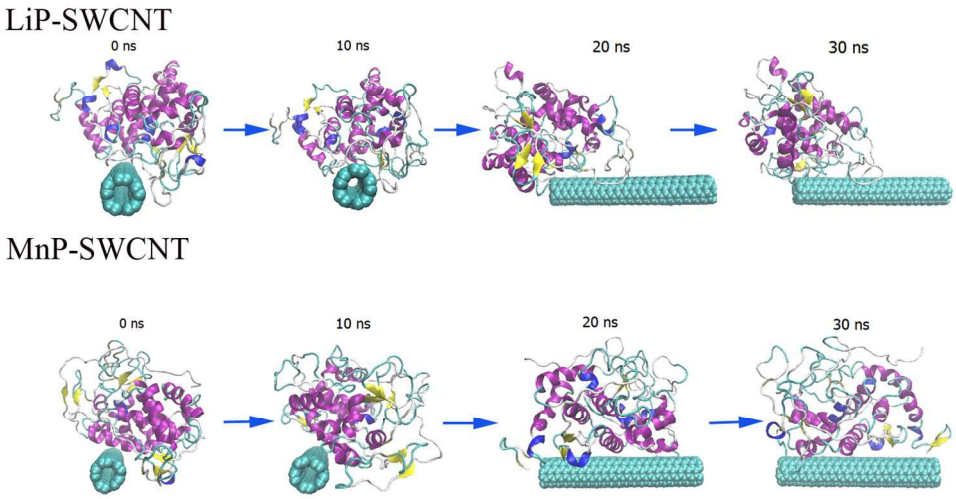

134x71mm (300 x 300 DPI)